Title

TMEM16F Forms a Ca2+-Activated Cation Channel Required for Lipid Scrambling in Platelets during Blood Coagulation

Journal

Cell, 151(1)

ISSN

0092-8674

Authors

Yang, Huanghe
Kim, Andrew
David, Tovo
et al.

Publication Date

2012-09-01

DOI

10.1016/j.cell.2012.07.036

Peer reviewed

Published in final edited form as:
Cell. 2012 September 28; 151(1): 111–122. doi:10.1016/j.cell.2012.07.036.

TMEM16F Forms a Ca^{2+}-Activated Cation Channel Required for Lipid Scrambling in Platelets during Blood Coagulation

Huanghe Yang[1,3], **Andrew Kim**[1,3], **Tovo David**[2], **Daniel Palmer**[2], **Taihao Jin**[1], **Jason Tien**[1], **Fen Huang**[1], **Tong Cheng**[1], **Shaun R. Coughlin**[2], **Yuh Nung Jan**[1], and **Lily Yeh Jan**[1,*]

[1]Departments of Physiology, Biochemistry, and Biophysics, Howard Hughes Medical Institute, University of California, San Francisco, San Francisco, CA 94143, USA

[2]Cardiovascular Research Institute, University of California, San Francisco, San Francisco, CA 94143, USA

SUMMARY

Collapse of membrane lipid asymmetry is a hallmark of blood coagulation. TMEM16F of the TMEM16 family that includes TMEM16A/B Ca^{2+}-activated Cl^- channels (CaCCs) is linked to Scott syndrome with deficient Ca^{2+}-dependent lipid scrambling. We generated TMEM16F knockout mice that exhibit bleeding defects and protection in an arterial thrombosis model associated with platelet deficiency in Ca^{2+}-dependent phosphatidylserine exposure and procoagulant activity and lack a Ca^{2+}-activated cation current in the platelet precursor megakaryocytes. Heterologous expression of TMEM16F generates a small-conductance Ca^{2+}-activated nonselective cation (SCAN) current with subpicosiemens single-channel conductance rather than a CaCC. TMEM16F-SCAN channels permeate both monovalent and divalent cations, including Ca^{2+}, and exhibit synergistic gating by Ca^{2+} and voltage. We further pinpointed a residue in the putative pore region important for the cation versus anion selectivity of TMEM16F-SCAN and TMEM16A-CaCC channels. This study thus identifies a Ca^{2+}-activated channel permeable to Ca^{2+} and critical for Ca^{2+}-dependent scramblase activity during blood coagulation.

INTRODUCTION

Phospholipids in the plasma membrane are asymmetric with phosphatidylcholine (PC) and sphingomyelin (SPH) predominantly in the outer leaflet, whereas phosphatidylethanolamine (PE) and phosphatidylserine (PS) are enriched in the inner leaflet. This asymmetry is maintained by substrate- and direction-specific transporters known as flippases and floppases (Contreras et al., 2010; Pomorski and Menon, 2006; van Meer, 2011). A third and the least understood category of lipid transporters is called scramblases, which can rapidly collapse the lipid asymmetry in a Ca^{2+}-dependent but energy-independent fashion, resulting in the exposure of PS to the cell surface (Bevers and Williamson, 2010; Sanyal and Menon, 2009; van Meer, 2011). This scramblase-mediated externalization of PS has important biological consequences in platelets, highly specialized hematopoietic cells that play a vital role in hemostasis and thrombosis. Platelets are accumulated at sites of vascular injury and are activated by exposed subendothelial factors such as collagen or by thrombin generated from the coagulation cascade pathway (Furie and Furie, 2008). Subsequent rise in the

*Correspondence: lily.jan@ucsf.edu.
[3]These authors contributed equally to this work

SUPPLEMENTAL INFORMATION
Supplemental Information includes Extended Experimental Procedures, six figures, and one table and can be found with this article online at http://dx.doi.org/10.1016/j.cell.2012.07.036.

cytoplasmic Ca^{2+} level triggers Ca^{2+}-activated lipid scrambling, thus exposing PS, which prompts the recruitment and activation of blood clotting factors—including factor V, factor X, and prothrombin—on the platelet surface (Bevers et al., 1983; Rosing et al., 1985).

Scott syndrome is a rare bleeding disorder with a defect in the Ca^{2+}-dependent phospholipid scrambling in the platelets, as well as erythrocytes and B lymphocyte cell lines derived from the patient (Zwaal et al., 2004). The first Scott syndrome patient reported in 1979 had frequent bouts of bleeding episodes associated with trauma or surgery, such as tooth extraction and tonsillectomy, and childbirth that subsequently required blood transfusion (Weiss et al., 1979). The patient displayed normal platelet counts and structure, platelet adhesion, platelet secretion, and aggregation but had a marked defect in platelet pro-coagulant activity due to reduction in the Ca^{2+}-dependent PS exposure, leading to reduced thrombin generation and defective coagulation. Recently, Suzuki and colleagues reported that the transmembrane protein with unknown function 16F (TMEM16F) is essential for the Ca^{2+}-dependent scramblase activity. Knockdown of TMEM16F in a B cell line results in a decrease in the rate of Ca^{2+} ionophore-induced PS and PE exposure, whereas TMEM16F overexpression strongly enhances PS exposure (Suzuki et al., 2010). DNA sequence analysis further demonstrates that Scott syndrome patients carry loss-of-function mutations in both *Tmem16F* alleles (Castoldi et al., 2011; Suzuki et al., 2010).

In the mammalian TMEM16 family (Figure 1A), TMEM16A and TMEM16B are Ca^{2+}-activated chloride channels (CaCCs) (Caputo et al., 2008; Schroeder et al., 2008; Yang et al., 2008) that are important for cellular functions ranging from fluid secretion and neuronal excitability to cancer progression (Ayoub et al., 2010; Huang et al., 2012; Stanich et al., 2011; Yang et al., 2008). The unexpected association of TMEM16F with Scott syndrome raises important questions about the function of TMEM16F, including: (1) whether it forms an ion channel and, if so, (2) what type of ion channel; (3) whether TMEM16F itself can scramble membrane lipids; (4) whether knocking out the mouse *Tmem16F* gene will cause defective blood coagulation; and (5) whether TMEM16F function in vivo is also important for thrombosis.

We have generated TMEM16F knockout mice exhibiting impaired hemostasis and decreased PS exposure on the surface of activated platelets, erythrocytes, and splenic B cells, resembling the major defects of Scott syndrome. Additionally, TMEM16F knockout mice showed a significant protection in an in vivo thrombosis assay, highlighting the importance of TMEM16F in the procoagulant state of platelets during thrombus formation. Surprisingly, loss of TMEM16F function resulted in the elimination of a Ca^{2+}-dependent cationic current in the platelet precursor megakaryocytes. Moreover, TMEM16F expressed in HEK293 cells and *Xenopus* as well as Axolotl oocytes gave rise to a small-conductance Ca^{2+}-activated nonselective cation (SCAN) channel more permeable to Ca^{2+} than other physiological cations. Importantly, mutagenesis of TMEM16F resulted in alterations of multiple properties, including ion selectivity and Ca^{2+} sensitivity, further supporting our conclusion that TMEM16F forms the SCAN channel. Thus, the discovery of TMEM16F as a Ca^{2+}-activated and Ca^{2+}-permeable nonselective cation channel crucial for Ca^{2+}-dependent lipid scrambling provides a new mechanistic insight into the blood coagulation pathway and a potential target for antithrombotic therapy.

RESULTS

TMEM16F Knockout Mice Are Defective in Ca^{2+}-Dependent Scramblase Activity and Display Impaired Hemostasis

To explore the physiological functions of TMEM16F, we generated TMEM16F knockout (KO) mice by deleting the second exon, leading to a frame-shift mutation of the *Tmem16F*

gene (Figures S1A–S1C available online) and the absence of TMEM16F protein in their platelets (Figure 1B). Homozygotes are viable, fertile, and without gross differences in morphology in comparison with wild-type (WT) mice.

To examine the impact of TMEM16F on the Ca^{2+}-dependent scramblase activity, we performed flow cytometry using the FITC-conjugated Annexin-V, a specific probe for PS exposure. The Ca^{2+} ionophore A23187 induced PS exposure from platelets, red blood cells (RBCs), and CD19+ splenic B cells but significantly less PS exposure for those cells without TMEM16F (Figures 1C and S1D–S1G). Similar to Scott syndrome patients, TMEM16F KO mice also showed impaired platelet procoagulant activity as measured by thrombin generation in platelet-rich plasma after addition of tissue factor (Figures 1D–1F) or factor XIIa (Figures S1H–S1J), whereas no significant difference was detected in platelet-poor plasma (Figures S1K to S1M). Moreover, TMEM16F KO mice exhibited prolonged bleeding time (167 ± 18 s) as compared with that of WT mice (97 ± 10 s, $p < 0.005$) (Figure 1G). The bleeding time of heterozygotes was normal, in agreement with the absence of disease manifestation of the children of a Scott syndrome patient (Bevers et al., 1983). To evaluate the effect of TMEM16F on thrombogenesis in vivo, we used 4% ferric chloride ($FeCl_3$) to induce occlusive thrombus formation in the carotid artery. Whereas seven out of eight WT mice showed cessation of flow within 20 min, all nine TMEM16F KO mice were fully protected from occlusion (Figure 1H). These findings underscore the important role of TMEM16F in mediating PS exposure for procoagulant activity leading to both hemostasis and thrombosis—a critical event in the arterial diseases associated with myocardial infarction and stroke as well as venous thromboembolic disorders (Furie and Furie, 2008).

A Ca^{2+}- and Voltage-Sensitive Outwardly Rectifying Current from Megakaryocytes of WT Mice, but Not TMEM16F KO Mice

For electrophysiological studies of the endogenous TMEM16F channel, bone marrow megakaryocytes proved to be an ideal cell type because: (1) megakaryocytes are the immediate precursors of platelets and share many molecular similarities and (2) megakaryocytes are easily recognizable among other bone marrow cells by their large size, distinct morphology, and ability to bind the megakaryocyte/platelet-specific cell surface marker CD41 (Figure 2A). The current was recorded with 140 mM NaCl on both sides of the inside-out membrane patch in order to minimize contaminations from Ca^{2+}-activated K^+ channels that are impermeable to both Cl^- and Na^+. We found that membrane patches from megakaryocytes of WT mice, but not TMEM16F KO mice, exhibited a Ca^{2+}-dependent outwardly rectifying current (Figures 2B–2E).

Heterologous Expression of TMEM16F Confirms that TMEM16F Gives Rise to a Ca^{2+}- and Voltage-Activated Ion Channel

To test whether TMEM16F forms a functional ion channel, we expressed the murine TMEM16F (mTMEM16F) in Axolotl oocytes (Figure 3) and HEK293 cells (Figure S2). Without endogenous CaCC (Figure 3B, left), Axolotl oocytes provide an expression system that enabled expression cloning of CaCC and characterization of TMEM16A-CaCC and TMEM16B-CaCC (Schroeder et al., 2008). The fluorescence signal indicative of surface expression of mTMEM16F fused with green fluorescence protein (TMEM16F-eGFP) peaked around 20 days after oocyte injection with cRNA (Figure 3A). Raising the internal Ca^{2+} induced time-dependent currents that were much larger at depolarized membrane potentials in recordings from inside-out patches from oocytes (Figure 3B and 3C) and mTMEM16F-transfected HEK293 cells (Figures S2B and S2C). Unlike TMEM16A-CaCC, which exhibits outward rectification at low internal Ca^{2+} concentrations but has a roughly linear current-voltage (*I-V*) relationship at higher internal Ca^{2+} concentrations (Figure S3A) —a characteristic of endogenous CaCC in many cell types (Hartzell et al., 2005), the

TMEM16F currents showed prominent outward rectification even at high internal Ca^{2+} concentrations (Figures 2, 3 and S2). We have further verified that TMEM16F forms this ion channel by performing mutagenesis studies reported in the later part of this study.

The TMEM16F Channel Is a Ca^{2+}-Activated Nonselective Cation Channel Rather Than a CaCC

Unexpectedly, we found that the TMEM16F channel is not a CaCC. By progressively reducing the NaCl concentration on the cytoplasmic side of the inside-out oocyte membrane patch while maintaining the external NaCl concentration at 140 mM, we found a drastic difference between mTMEM16A-CaCC and the mTMEM16F-induced current (Figures 4A, S3A, and S3B). Whereas it caused a leftward shift of the reversal potential for mTMEM16A-CaCC (Figure S3A) indicative of a chloride channel with a permeability ratio P_{Na}/P_{Cl} of ~0.14 (Figure 4A), the reversal potential for the mTMEM16F-induced current shifted to the right instead (Figure S3B), revealing a permeability ratio P_{Na}/P_{Cl} of ~7 (Figure 4A).

To further validate that mTMEM16F gives rise to a Ca^{2+}-activated cation channel, we recorded from membrane patches excised from mTMEM16F-expressing Axolotl oocytes and megakaryocytes of WT mice. The Ca^{2+}- and voltage-activated, time-dependent current persisted even with isotonic 140 mM sodium methanesulfonate (MES) on both sides of the membrane (Figures 4B and 4C). Because the large anion MES is poorly permeable through chloride channels (Frings et al., 2000), this current is most likely carried by Na^+ ions. The cation permeability was confirmed by monitoring the reversal potential when the intracellular solution was switched from 140 mM NaCl to 140 mM NaMES for TMEM16F-expressing Axolotl oocytes (Figure S3C) and for megakaryocytes with endogenous TMEM16F channels (Figure S3D).

To assess the permeability to other cations, we measured the reversal potential under bi-ionic conditions for TMEM16F expressed in heterologous systems (Figures S3E, S3F, 4D, and 4E) and endogenous TMEM16F in megakaryocytes (Figures S3D and 4D). The TMEM16F channel is almost equally permeable to Li^+, Na^+, K^+, Rb^+, and Cs^+ but much more permeable to Ca^{2+} and Ba^{2+} (Figure 4E) and has a large pore (~6 Å radius) permeable to cations as large as N-methyl-D-glucamine (NMDG, Figures 4E, S3D, and S3F) and tetraethylammonium (TEA, Figure 4E). Indeed, the outwardly rectifying currents persisted in solutions containing NMDG or TEA as the cation and MES as the anion on both sides of the membrane (Figures S3G and S3H) or when both sides of the membrane patch were exposed to isotonic 70 mM $Ca(MES)_2$ solutions (Figure 4F). Thus, TMEM16F expression yielded a Ca^{2+}-activated nonselective cation (CAN) channel that is more permeable to Ca^{2+} than monovalent cations.

We further expressed mTMEM16F in *Xenopus* oocytes, which normally display CaCC, but not CAN, currents (Figure S4A), and replaced Cl^- with MES to eliminate the CaCC currents. The mTMEM16F channels were readily expressed on the *Xenopus* oocyte surface (Figure S4B), and the resulting current (Figures S4C–S4H) resembled every aspect of the current in Axolotl oocytes and HEK293 cells expressing TMEM16F as well as the endogenous TMEM16F current in megakaryocytes: Ca^{2+} and voltage activated and nonselectively permeable to large cations and Ca^{2+}.

TMEM16F Is a Small-Conductance Ca^{2+}-Activated Nonselective Cation Channel

A hallmark of CAN channels is a single-channel conductance of 15–35 pS (Teulon, 2000). Using noise analysis, we estimated the single channel conductance of TMEM16F channels (Figures 5A and 5B) to be $\gamma = 0.45 \pm 0.07$ pS (n = 15). The small single-channel

conductance, as well as the high Ca^{2+} selectivity and the synergistic gating by Ca^{2+} and voltage, distinguishes TMEM16F from most of the known CAN channels. We therefore named TMEM16F channels as "SCAN channels," for "small-conductance Ca^{2+}-activated nonselective cation channels."

The TMEM16F-SCAN channel is also distinct from the known CAN and CaCC channels in its pharmacological profile. Whereas cytoplasmic application of 300 μM niflumic acid (NFA) readily blocked the TMEM16A-CaCC current, it had no effect on TMEM16F-SCAN current in Axolotl oocytes, *Xenopus* oocytes, or HEK293 cells (Figures 5C, 5D, S5A, S5C, and S5D). Inclusion of NFA in the external solution also failed to block TMEM16F-SCAN channels (Figure S5A) even though this same treatment readily blocked the endogenous CaCC in *Xenopus* oocytes (data not shown). Likewise, two other common blockers for both CaCC and CAN channels (Hartzell et al., 2005; Teulon, 2000; Ullrich et al., 2005), flufenamic acid (FFA) and 5-nitro-2-(3-phenylpropylamino)-benzoate (NPPB), blocked the endogenous CaCC in *Xenopus* oocytes, but not the TMEM16F-SCAN channels expressed in Axolotl or *Xenopus* oocytes (Figures S5B and S5C). We also tested the effects of nucleotides, which inhibit a subset of the CAN channels (Nilius et al., 2004; Teulon, 2000; Ullrich et al., 2005). Cytoplasmic application of 2 mM AMP or ATP did not inhibit the TMEM16F-SCAN current (Figure 5E). We further tested the effects of some nonselective cation channel blockers (Peña and Ordaz, 2008) and found that cytoplasmic application of 100 μM Ruthenium red (Ru-Red), 2-Aminoethyl diphenylborinate (2APB), Cd^{2+}, or Gd^{3+} inhibited the mTMEM16F channels, whereas N-Phenylanthranilic acid (NPC) and SKF96365 had no effect (Figure S5D). Thus, the TMEM16F-SCAN channel can be blocked by some non-specific cation channel blockers such as Gd^{3+}, Cd^{2+}, 2APB, and Ruthenium red but is pharmacologically distinct from the CaCC channels and known CAN channels that are sensitive to NFA, FFA, NPPB, DPC, or nucleotides.

Identification of a Residue Important for the Cation versus Anion Selectivity of TMEM16F-SCAN and TMEM16A-CaCC Channels

In a search for residues that are different in the putative pore region of TMEM16F-SCAN and TMEM16A-CaCC channels, we found a position in the transmembrane segment TM5 that is occupied by lysine in all known anion channels, namely TMEM16A-CaCC and TMEM16B-CaCC. In contrast, this position is occupied by glutamine in the cation channel (Q559 in mTMEM16F-SCAN) (Figure 6A). With lysine substitution for Q559, the Q559K mutant mTMEM16F channel exhibited much slower activation kinetics (Figures 6B and 6C) and was less selective to Na^+ ($P_{Na}/P_{Cl} = 2.2$ compared to WT control of $P_{Na}/P_{Cl} = 6.8$) (Figures 6D, 6F, and 6G). In contrast, the K584Q mutant mTMEM16A channel was less permeable to Cl^- ($P_{Cl}/P_{Na} = 4.1$ compared to WT control of $P_{Cl}/P_{Na} = 7.0$) (Figures 6E–6G). These mutagenesis experiments have therefore identified a key residue near the N-terminal end of TM5 that is important for the ion selectivity of two closely related TMEM16 channel family members that form channels with preference for ions of opposite charge.

Characterization of the Ca^{2+}- and Voltage-Dependent Activation of TMEM16F-SCAN Channels

We found that increasing internal Ca^{2+} accelerated channel activation and increased channel open probability (Figure 7A) and caused a shift of the *G-V* curve for the voltage dependence of the mTMEM16F channels expressed in HEK293 cells to more negative voltages (Figures 7B and S6F and Table S1). The apparent Ca^{2+} dissociation constant (K_D) dropped from 10.8 μM to 3.4 μM (an increase in Ca^{2+} sensitivity) ($p < 0.01$) when the membrane potential was depolarized from +60 to +180 mV (Figure 7C). This synergistic gating of mTMEM16F channels by internal Ca^{2+} and voltage bears some resemblance to the gating of the BK-type Ca^{2+}-activated K^+ channels that belong to the family of voltage-gated K^+ channels

(Magleby, 2003), except for the apparent requirement for internal Ca^{2+} to activate TMEM16F channels—a protein with eight trans-membrane segments without any canonical voltage-sensing domains. The Hill coefficients for Ca^{2+} activation of TMEM16F channels are between 2 and 3, suggesting that multiple Ca^{2+} ions may bind to the channel and they work cooperatively to activate the channel.

The Hartzell laboratory recently identified two acidic residues (E702 and E705) in TMEM16A-CaCC that are important for the Ca^{2+}-dependent channel activation (Yu et al., 2012). To test whether the equivalent residues are also important for the Ca^{2+}-dependent activation of the TMEM16F-SCAN channel, we replaced these acidic residues with glutamine. Because the E670Q mutation of TMEM16F greatly reduced surface expression, we concentrated our study on the E667Q mutation. The apparent Ca^{2+} sensitivity of the E667Q mutant TMEM16F channel was markedly reduced (Figure 7D and 7E); the EC_{50} of the mutant channel (2.8 mM) at +60 mV was about 2,000-fold higher than that of the WT channel (13.6 μM). It thus appears that TMEM16F-SCAN and TMEM16A-CaCC might share a conserved mechanism for Ca^{2+}-dependent channel gating.

To test whether alkaline earth metals other than Ca^{2+} can also activate TMEM16F channels, we exposed inside-out membrane patches excised from Axolotl or *Xenopus* oocytes to Mg^{2+} and Sr^{2+} (Figures S6A to S6C). We found that Sr^{2+} also activated the mTMEM16F channels, whereas 500 μM Mg^{2+} failed to activate these channels.

Prompted by the report that the D409G mutation of TMEM16F enhances the Ca^{2+}-dependent scramblase activity so that PS exposure takes place at the basal internal Ca^{2+} level in a B cell line (Suzuki et al., 2010), we expressed this mutant channel in HEK293 cells and found it to be less active than the WT TMEM16F channel, as evidenced by a shift of the half-activation voltage ($V_{1/2}$) to more depolarizing voltages (Figure S6E and Table S1) and a decrease of the apparent Ca^{2+} sensitivity (Figures S6D and S6F). The Ca^{2+} permeability of WT and D409G mutant TMEM16F channels was comparable (Figure S6G). Moreover, overexpression of WT or D409G mutant TMEM16F-SCAN channels in HEK293 cells did not cause any obvious Ca^{2+}-induced PS exposure (Figure S6H). Taken together, these observations are compatible with the scenario that some factors in blood cells act together with TMEM16F to mediate the Ca^{2+}-dependent scramblase activity.

Interestingly, the apparent Ca^{2+} sensitivity of the endogenous TMEM16F channels in megakaryocytes is greater than that of heterologously expressed mTMEM16F channels at certain voltages, as evidenced by the leftward shift of the Ca^{2+} dose-response curve (Figure 7F and 7G). The greater Ca^{2+} sensitivity of the endogenous TMEM16F channels further suggests that there may be regulatory factors in native cells that make the endogenous TMEM16F channels more active.

DISCUSSION

In this study, we report that TMEM16F, which is linked to Scott syndrome and belongs to the TMEM16 family that includes TMEM16A and TMEM16B CaCCs, forms a SCAN channel with considerable Ca^{2+} selectivity—an unprecedented finding of a cation channel as a closely related family member of anion channels. We have further generated TMEM16F KO mice to show that they recapitulate the defective Ca^{2+}-activated scramblase activity in platelets, B cells, and red blood cells that are characteristic of Scott syndrome. Not only is the reduction of PS exposure associated with prolonged bleeding, the loss of TMEM16F function greatly reduced the propensity to thrombosis.

TMEM16F Forms a SCAN Channel

Our conclusion that TMEM16F gives rise to SCAN channels is supported by the following evidence: (1) SCAN channels are generated by expressing TMEM16F in three different heterologous expression systems; (2) mutation of a residue in the transmembrane domain of TMEM16F alters SCAN channel properties, including ion selectivity; (3) mutation of an acidic residue of TMEM16F that corresponds to a putative Ca^{2+} binding residue in TMEM16A-CaCC reduces the Ca^{2+} sensitivity of SCAN channels; and (4) an endogenous Ca^{2+}-activated cation channel with similar properties is present in megakaryocytes from WT, but not TMEM16F KO mice.

The residue that is important for the cation selectivity of TMEM16F-SCAN and the anion selectivity of TMEM16A-CaCC resides near the N-terminal end of the fifth transmembrane segment (TM5) in the putative pore region; swapping this residue rendered the Q559K-TMEM16F channel more permeable to Cl^- and the K584Q-TMEM16A channel more permeable to Na^+. Unlike the mutagenesis of this key residue identified in our study, mutations reported to alter ion selectivity in previous studies target residues that are identical in TMEM16A and TMEM16F (Yang et al., 2008), a finding that has not been replicated in a recent study (Yu et al., 2012).

Features that distinguish TMEM16F-SCAN channels from most of the Ca^{2+}-activated nonselective cation (CAN) channels (Teulon, 2000) include the ability to permeate Ca^{2+} ions ($P_{Ca}/P_{Na} = 2.6$), the small single-channel conductance (~0.45 pS), the synergistic gating by Ca^{2+} and voltage, and the distinct pharmacological characteristics. Although TRPM4 and TRPM5, two recently identified CAN channels (Hofmann et al., 2003; Launay et al., 2002; Prawitt et al., 2003), also show some voltage dependence, they are clearly different from the TMEM16F-SCAN channels in other key aspects: TRPM4-CAN and TRPM5-CAN channels are impermeable to divalent cations, have much larger single-channel conductance (15–25 pS), and are sensitive to intracellular adenosine nucleotides and FFA (Hofmann et al., 2003; Prawitt et al., 2003; Ullrich et al., 2005).

Conflicting conclusions regarding the biophysical properties of TMEM16F have been drawn in recent studies. Three papers from the same laboratory identified TMEM16F as a volume-regulated anion channel (Almaça et al., 2009), a Ca^{2+}-activated chloride channel (Schreiber et al., 2010), and an outwardly rectifying chloride channel (Martins et al., 2011). These three types of channels are different from one another, though they are all anion channels. In contrast, our studies of TMEM16F channels in megakaryocytes and three different expression systems clearly reveal that TMEM16F forms a small-conductance Ca^{2+}-activated nonselective cation channel with minimal anion permeability (P_{Na}/P_{Cl} is ~7). Another study reports an inability of TMEM16F to target to the HEK293 cell membrane and a lack of current detected using whole-cell patch clamp (Duran et al., 2012), which may be accounted for by the lower intracellular Ca^{2+} concentration used in that study. The identification in our study of a residue that is important for the ion selectivity and kinetic properties of the TMEM16F-SCAN channel further supports the notion that TMEM16F is a bona fide ion channel that prefers permeating cations, including Ca^{2+}.

TMEM16F Is Important for Ca^{2+}Dependent PS Exposure for Coagulation and Thrombosis

Following studies of Scott syndrome patients and immortalized blood cell lines that led to the identification of TMEM16F as the culprit (Castoldi et al., 2011; Suzuki et al., 2010), we have generated TMEM16F KO mice to demonstrate that TMEM16F is important for the Ca^{2+}-dependent scramblase activity in blood cells and for thrombin generation. Not only do TMEM16F KO mice show impaired hemostasis as evidenced by the prolonged bleeding time, our study of carotid artery thrombus formation has revealed that TMEM16F is also

crucial for thrombosis. These TMEM16F KO mice thus provide a suitable mouse model to help understand the physiological and pathophysiological mechanism of hemostasis and thrombosis.

How might the TMEM16F-SCAN channel contribute to the Ca^{2+}-dependent scramblase activity? There are conceivably three possible scenarios. First, the influx of Ca^{2+} through TMEM16F-SCAN channels may directly activate a yet undefined scramblase that may be associated with TMEM16F-SCAN channels. Ca^{2+} influx through Ca^{2+}-permeable channels, such as store-operated Ca^{2+} channels (Varga-Szabo et al., 2011) and nucleotide-activated P2X1 channels (Mahaut-Smith et al., 2011) that can promote lipid scrambling in platelets, could increase the local Ca^{2+} concentrations to activate TMEM16F-SCAN channels, which permeate Ca^{2+}, thereby triggering a positive feedback to facilitate Ca^{2+} entry, and their very small single-channel conductance could limit the extent of Ca^{2+} influx, thereby reducing energy expenditure and the risk of toxicity. Second, TMEM16F-SCAN channels may act as a Ca^{2+}-sensitive regulator of an undefined scramblase; in this scenario, removal of TMEM16F genetically could impair the efficiency of scramblase activation or compromise scramblase maturation or traffic to the cell membrane. Third, the TMEM16F-SCAN channel may be a multitasking or multifunctional moonlighting protein such as opsin (Menon et al., 2011) and can carry out two distinct tasks: transporting ions and scrambling phospholipids. Conformational changes induced by Ca^{2+} binding to the TMEM16F-SCAN channel might facilitate the formation of transient membrane defects such as water pores in the lipid-channel interface. These transient membrane defects could facilitate fast translocation of the various charged headgroups of phospholipids across the membrane, thereby disrupting the membrane lipid asymmetry (Gurtovenko et al., 2010; Sanyal and Menon, 2009). Our study thus far is consistent with the hypothesis that TMEM16F is important, but not sufficient, for the Ca^{2+}-dependent scramblase activity.

Given the uncertainty of molecular identity of scramblase and the complexity of the lipid scrambling machinery in blood cells (Bevers and Williamson, 2010), it is difficult to pinpoint the exact role of the TMEM16F-SCAN channel in lipid scrambling. Nevertheless, a few insights can be gained from our current study: (1) The platelets of TMEM16F KO mice exhibit significantly reduced but still substantial Ca^{2+}-induced PS exposure when treated with high concentrations of the Ca^{2+} ionophore A23187 (Figures 1C, S1E, and S1F). This implies that either the Ca^{2+} influx through TMEM16F-SCAN channels or conformational changes during channel activation directly activates an unknown scramblase; or alternatively, if TMEM16F itself is one of the scramblases, there might be other unknown scramblase(s) mediating the remaining Ca^{2+}-induced PS exposure in platelets without TMEM16F. (2) In contrast to the enhanced scramblase activity when TMEM16F is expressed in Ba/F3 cells (Suzuki et al., 2010) or lymphoma cells (Segawa et al., 2011), overexpression of WT or D409G mutant TMEM16F in HEK293 cells did not cause Ca^{2+}-induced PS exposure (Figure S6H), though it remains possible that cell-type-specific regulation renders TMEM16F capable of translocating phospholipids in blood cells. (3) Although the D409G mutant TMEM16F drastically increases the Ca^{2+} sensitivity of lipid scrambling when expressed in a B cell line (Suzuki et al., 2010), the Ca^{2+} sensitivity and Ca^{2+} permeability of D409G mutant TMEM16F channels expressed in HEK293 cells are not enhanced (Figure S6). It seems more likely that the D409G mutation facilitates PS exposure by altering TMEM16F interaction with other components of a putative scramblase complex or by enhancing the efficiency of TMEM16F to scramble phospholipids.

Consistent with our studies of HEK293 cells, many nonhematopoietic cell lines, including CHO, BHK, 3T3, MCF-7, and HeLa, display no Ca^{2+}-activated scramblase activity (Williamson et al., 2007). Because TMEM16F is expressed in many different mouse tissues (Schreiber et al., 2010), it remains to be examined whether nonhematopoietic primary cells

that express TMEM16F exhibit Ca^{2+}-induced PS exposure and whether other functions unrelated to lipid scrambling are altered in TMEM16F KO mice.

In conclusion, our finding of TMEM16F as a SCAN channel with considerable Ca^{2+} permeability, the presence of functional TMEM16F-SCAN channels in megakaryocytes, as well as the generation of TMEM16F KO mice with reduced thrombosis and blood coagulation deficits that are characteristic of Scott syndrome will greatly facilitate future studies to elucidate the molecular mechanism for phospholipid scrambling in blood cells. The TMEM16F-SCAN channels discovered in this study hence might serve as a new pharmaceutical target to treat human hemostatic and thrombotic disorders, such as stroke and heart attack.

EXPERIMENTAL PROCEDURES

Additional information regarding plasmids, TMEM16F KO mouse generation, and detailed procedures for flow cytometry, electrophysiology, and in vivo experiments are described in the Supplemental Information. All animal procedures were approved by the UCSF Institutional Animal Care and Use Committee and were performed according to the guidelines provided.

Generation of TMEM16F Knockout Mice

Using recombineering technology, loxP site was inserted in the 3′ intronic region of exon 2 and a frt-neo-frt-loxP cassette was inserted in the 5′ intronic region of exon 2. Linearized targeting vector was electroporated into embryonic stem cells. G418 and Gancyclovir were used in the ES cell media to select for ES cell clones with proper homologous recombination, which were confirmed by Southern blot analysis. Correctly targeted ES cells were then injected into blastocysts, and germline transmission was confirmed by PCR. The resulting mouse was bred with β-Actin-Flp mouse to delete neomycin cassette. Male β-Actin-Cre deleter mice were then bred with female TMEM16F flox/+ neomycin-deleted mice to generate founding TMEM16F heterozygous mice. TMEM16F heterozygous mice (het) were crossed with each other to generate TMEM16F KO mice. PCR genotyping was performed on tail DNA extracted from such offsprings. All experimental mice were backcrossed between two and five generations to C57Bl6.

Immunoblotting of Washed Mouse Platelet Lysates

Blood was collected from the vena cava of anesthetized mice in ACD (2.5 g Trisodium citrate, 1.37 g citric acid monohydrate, 2.0 g dextrose in 100 ml of ddH_2O), mixed with 20 mM PIPES in saline (pH 6.5), and centrifuged at 100 × *g* in room temperature. The platelet-containing upper phase was mixed with low-pH washing buffer (140 mM NaCl, 10 mM $NaHCO_3$, 2.5 mM KCl, 0.5 mM Na_2HPO_4, 1 mM $MgCl_2$, 22 mM Trisodium Citrate, 0.1% dextrose, and 0.35% BSA [pH 6.5]) with 3 U/ml apyrase (Sigma) and then centrifuged at 500 × *g* at room temperature. Pelleted platelets were resuspended in Ca^{2+}-free Tyrode's HEPES (CFTH) buffer (134 mM NaCl, 12 mM $NaHCO_3$, 2.9 mM KCl, 0.34 mM Na_2HPO_4, 1.0 mM $MgCl_2$, 10 mM HEPES, 0.9% wt/vol dextrose, and 0.35% wt/vol BSA [pH 7.4]) then lysed using RIPA buffer. Western blot analysis was performed using a rabbit polyclonal antibody raised against a peptide corresponding to the N terminus of mouse TMEM16F protein. The β-actin antibody was used as loading control.

Flow Cytometric Analysis of PS Exposure

To assess the A23187 Ca^{2+} ionophore-induced PS exposure on the platelet surface, 1×10^6 platelets were resuspended in 24 μl total volume of CFTH buffer with 2 mM Ca^{2+} with or without A23187 (Sigma-Aldrich). This was immediately followed by addition of 1 μl FITC-

conjugated Annexin-V (BD Biosciences) and incubation in 37°C water bath for 30 min. The incubation was quenched using 500 μl of chilled CFTH buffer, and platelets were analyzed using FACSCalibur (Becton Dickinson). Red blood cells were collected from the lower phase following whole-blood centrifugation and were similarly used for flow cytometric analysis.

For B cell analysis, mouse spleens from WT and KO mice were gently mashed, filtered, and washed once using PBS. The cells (1×10^6) were resuspended in 1X Annexin-V binding buffer (BD Biosciences) and were incubated with A23187 in 37°C water bath for 15 min. Cells were subsequently stained using Annexin-V FITC and CD19 APC on ice for 15 min followed by 500 μl of annexin-V binding buffer containing 7-AAD (1 μg/ml final).

Thrombin Generation Measured by a Thrombinoscope

Thrombin generation was measured using a fluorogenic thrombin substrate on a multiwell automated fluorescent plate reader (ThrombinoSCOPE, Maastricht, The Netherlands).

Tail-Bleeding Assay

A small tip (1–2 mm) of the tail was transected and immersed in 37°C saline water. The time for the bleeding to stop was measured up to 5 min. For mice bleeding more than 5 min, pressure was applied near the wound to stop the bleeding. The mice were genotyped after the experiment. Statistical significance was determined with the Student's t test.

$FeCl_3$-Induced Carotid Thrombosis Model

Eight- to fourteen-week-old mice were anesthetized. The carotid was dissected free, a flow probe was placed around the left common carotid artery proximal to the bifurcation, and the artery was exposed to filter papers soaked in $FeCl_3$ for 3 min. Arterial flow was measured continuously until clotting occurred (defined as no flow for ≥ 2 min). If no stoppage occured, measurements were ceased at 20 min. Percentage of arteries without occlusion (i.e., with continued flow) at the end of the assay was determined. Kaplan-Meier-type data were compared by log rank test.

Molecular Biology and Channel Expression

cRNA (5–100 ng) was injected into defolliculated oocytes. HEK293 cells were transfected with corresponding plasmids using FuGENE6 (Roche) and were cultured for 1–3 days before recording.

Confocal Imaging

Axolotl or *Xenopus* oocytes were stained with 50 μg/ml Alexa-633-conjugated Concanavalin A for 15 min at room temperature. TMEM16F-eGFP proteins in HEK293 cells were detected using Alexa-488-conjugated anti-rabbit antibody. All images were acquired using a Leica SP5 laser confocal microscope.

Electrophysiology and Data Analysis

Macroscopic currents were recorded from inside-out patches. Data were acquired using an Axopatch 200-B patch-clamp amplifier and pClamp9 software (Molecular Devices). All experiments were performed at room temperature (22°C –24°C).

To determine the reversal potentials while the NaCl concentration of the internal solution (without buffer) was varied, the osmolality of each solution was adjusted to about 330 mOsm/kg by addition of sucrose, except for the 280 mM and 420 mM NaCl solutions, which had higher osmolalities and contained no sucrose. To minimize leak currents, patches

with seal resistance lower than 3 GΩ were discarded. Similar reversal potential values were obtained by two different protocols (mTMEM16F in Figure 4A with the ramp protocol and Figure 6F with the voltage-step protocol).

For noise analysis, the currents were recorded at +80 mV using a gap-free protocol. The data were filtered at 1 KHz with an eight-pole low-pass Bessel filter were and sampled at 5 KHz.

For megakaryocyte recording, we used a protocol adopted from that of Mahaut-Smith (Mahaut-Smith, 2004).

Clampfit10 (Molecular Devices) and Origin (OriginLab) were used for data analysis.

Supplementary Material

Refer to Web version on PubMed Central for supplementary material.

Acknowledgments

We thank David Gorczyca for help with confocal imaging; Xiuming Wong for help with cell culture; and Jianmin Cui, Ehud Isacoff, Min Li, Shi-Bing Yang, James Berg, and Christian Peters for suggestions and comments on the manuscript. We also thank Kevin Shannon and Ethan Weiss for sharing their CBC machine, Thrombinoscope, and other equipment. This study was supported by the NIH grant HL65185 to S.R.C. and MH65334 to L.Y.J. Y.N.J. and L.Y.J. are Howard Hughes Medical Institute investigators.

References

Almaça J, Tian Y, Aldehni F, Ousingsawat J, Kongsuphol P, Rock JR, Harfe BD, Schreiber R, Kunzelmann K. TMEM16 proteins produce volume-regulated chloride currents that are reduced in mice lacking TMEM16A. J Biol Chem. 2009; 284:28571–28578. [PubMed: 19654323]

Ayoub C, Wasylyk C, Li Y, Thomas E, Marisa L, Robé A, Roux M, Abecassis J, de Reyniès A, Wasylyk B. ANO1 amplification and expression in HNSCC with a high propensity for future distant metastasis and its functions in HNSCC cell lines. Br J Cancer. 2010; 103:715–726. [PubMed: 20664600]

Bevers EM, Williamson PL. Phospholipid scramblase: an update. FEBS Lett. 2010; 584:2724–2730. [PubMed: 20302864]

Bevers EM, Comfurius P, Zwaal RF. Changes in membrane phospholipid distribution during platelet activation. Biochim Biophys Acta. 1983; 736:57–66. [PubMed: 6418205]

Caputo A, Caci E, Ferrera L, Pedemonte N, Barsanti C, Sondo E, Pfeffer U, Ravazzolo R, Zegarra-Moran O, Galietta LJ. TMEM16A, a membrane protein associated with calcium-dependent chloride channel activity. Science. 2008; 322:590–594. [PubMed: 18772398]

Castoldi E, Collins PW, Williamson PL, Bevers EM. Compound heterozygosity for 2 novel TMEM16F mutations in a patient with Scott syndrome. Blood. 2011; 117:4399–4400. [PubMed: 21511967]

Contreras FX, Sánchez-Magraner L, Alonso A, Goñi FM. Transbilayer (flip-flop) lipid motion and lipid scrambling in membranes. FEBS Lett. 2010; 584:1779–1786. [PubMed: 20043909]

Duran C, Qu Z, Osunkoya AO, Cui Y, Hartzell HC. ANOs 3-7 in the anoctamin/Tmem16 Cl− channel family are intracellular proteins. Am J Physiol Cell Physiol. 2012; 302:C482–C493. [PubMed: 22075693]

Frings S, Reuter D, Kleene SJ. Neuronal Ca^{2+} -activated Cl^{-} channels—homing in on an elusive channel species. Prog Neurobiol. 2000; 60:247–289. [PubMed: 10658643]

Furie B, Furie BC. Mechanisms of thrombus formation. N Engl J Med. 2008; 359:938–949. [PubMed: 18753650]

Gurtovenko AA, Anwar J, Vattulainen I. Defect-mediated trafficking across cell membranes: insights from in silico modeling. Chem Rev. 2010; 110:6077–6103. [PubMed: 20690701]

Hartzell C, Putzier I, Arreola J. Calcium-activated chloride channels. Annu Rev Physiol. 2005; 67:719–758. [PubMed: 15709976]

Hofmann T, Chubanov V, Gudermann T, Montell C. TRPM5 is a voltage-modulated and Ca($^{2+}$)-activated monovalent selective cation channel. Curr Biol. 2003; 13:1153–1158. [PubMed: 12842017]

Huang WC, Xiao S, Huang F, Harfe BD, Jan YN, Jan LY. Calcium-activated chloride channels (CaCCs) regulate action potential and synaptic response in hippocampal neurons. Neuron. 2012; 74:179–192. [PubMed: 22500639]

Launay P, Fleig A, Perraud AL, Scharenberg AM, Penner R, Kinet JP. TRPM4 is a Ca^{2+}-activated nonselective cation channel mediating cell membrane depolarization. Cell. 2002; 109:397–407. [PubMed: 12015988]

Magleby KL. Gating mechanism of BK (Slo1) channels: so near, yet so far. J Gen Physiol. 2003; 121:81–96. [PubMed: 12566537]

Mahaut-Smith MP. Patch-clamp recordings of electrophysiological events in the platelet and megakaryocyte. Methods Mol Biol. 2004; 273:277–300. [PubMed: 15308807]

Mahaut-Smith MP, Jones S, Evans RJ. The P2X1 receptor and platelet function. Purinergic Signal. 2011; 7:341–356. [PubMed: 21484087]

Martins JR, Faria D, Kongsuphol P, Reisch B, Schreiber R, Kunzelmann K. Anoctamin 6 is an essential component of the outwardly rectifying chloride channel. Proc Natl Acad Sci USA. 2011; 108:18168–18172. [PubMed: 22006324]

Menon I, Huber T, Sanyal S, Banerjee S, Barré P, Canis S, Warren JD, Hwa J, Sakmar TP, Menon AK. Opsin is a phospholipid flippase. Curr Biol. 2011; 21:149–153. [PubMed: 21236677]

Nilius B, Prenen J, Voets T, Droogmans G. Intracellular nucleotides and polyamines inhibit the Ca^{2+}-activated cation channel TRPM4b. Pflugers Arch. 2004; 448:70–75. [PubMed: 14758478]

Peña F, Ordaz B. Non-selective cation channel blockers: potential use in nervous system basic research and therapeutics. Mini Rev Med Chem. 2008; 8:812–819. [PubMed: 18673137]

Pomorski T, Menon AK. Lipid flippases and their biological functions. Cell Mol Life Sci. 2006; 63:2908–2921. [PubMed: 17103115]

Prawitt D, Monteilh-Zoller MK, Brixel L, Spangenberg C, Zabel B, Fleig A, Penner R. TRPM5 is a transient Ca^{2+}-activated cation channel responding to rapid changes in $[Ca^{2+}]_i$. Proc Natl Acad Sci USA. 2003; 100:15166–15171. [PubMed: 14634208]

Rosing J, van Rijn JL, Bevers EM, van Dieijen G, Comfurius P, Zwaal RF. The role of activated human platelets in prothrombin and factor X activation. Blood. 1985; 65:319–332. [PubMed: 3967085]

Sanyal S, Menon AK. Flipping lipids: why an' what's the reason for? ACS Chem Biol. 2009; 4:895–909. [PubMed: 19689162]

Schreiber R, Uliyakina I, Kongsuphol P, Warth R, Mirza M, Martins JR, Kunzelmann K. Expression and function of epithelial anoctamins. J Biol Chem. 2010; 285:7838–7845. [PubMed: 20056604]

Schroeder BC, Cheng T, Jan YN, Jan LY. Expression cloning of TMEM16A as a calcium-activated chloride channel subunit. Cell. 2008; 134:1019–1029. [PubMed: 18805094]

Segawa K, Suzuki J, Nagata S. Constitutive exposure of phosphatidylserine on viable cells. Proc Natl Acad Sci USA. 2011; 108:19246–19251. [PubMed: 22084121]

Stanich JE, Gibbons SJ, Eisenman ST, Bardsley MR, Rock JR, Harfe BD, Ordog T, Farrugia G. Ano1 as a regulator of proliferation. Am J Physiol Gastrointest Liver Physiol. 2011; 301:G1044–G1051. [PubMed: 21940901]

Suzuki J, Umeda M, Sims PJ, Nagata S. Calcium-dependent phospholipid scrambling by TMEM16F. Nature. 2010; 468:834–838. [PubMed: 21107324]

Teulon, J. Ca^{2+}-activated non-selective cation channels. In: Endo, M.; Kurachi, Y.; Mishina, M., editors. Pharmacology of ionic channel function: activators and inhibitors. New York: Springer-Verlag; 2000. p. 625-649.

Ullrich ND, Voets T, Prenen J, Vennekens R, Talavera K, Droogmans G, Nilius B. Comparison of functional properties of the Ca^{2+}-activated cation channels TRPM4 and TRPM5 from mice. Cell Calcium. 2005; 37:267–278. [PubMed: 15670874]

van Meer G. Dynamic transbilayer lipid asymmetry. Cold Spring Harb Perspect Biol. 2011; 3:a004671. [PubMed: 21436058]

Varga-Szabo D, Braun A, Nieswandt B. STIM and Orai in platelet function. Cell Calcium. 2011; 50:270–278. [PubMed: 21616531]

Weiss HJ, Vicic WJ, Lages BA, Rogers J. Isolated deficiency of platelet procoagulant activity. Am J Med. 1979; 67:206–213. [PubMed: 572637]

Williamson P, Halleck MS, Malowitz J, Ng S, Fan X, Krahling S, Remaley AT, Schlegel RA. Transbilayer phospholipid movements in ABCA1-deficient cells. PLoS ONE. 2007; 2:e729. [PubMed: 17710129]

Yang YD, Cho H, Koo JY, Tak MH, Cho Y, Shim WS, Park SP, Lee J, Lee B, Kim BM, et al. TMEM16A confers receptor-activated calcium-dependent chloride conductance. Nature. 2008; 455:1210–1215. [PubMed: 18724360]

Yu K, Duran C, Qu Z, Cui YY, Hartzell HC. Explaining calcium-dependent gating of anoctamin-1 chloride channels requires a revised topology. Circ Res. 2012; 110:990–999. [PubMed: 22394518]

Zwaal RF, Comfurius P, Bevers EM. Scott syndrome, a bleeding disorder caused by defective scrambling of membrane phospholipids. Biochim Biophys Acta. 2004; 1636:119–128. [PubMed: 15164759]

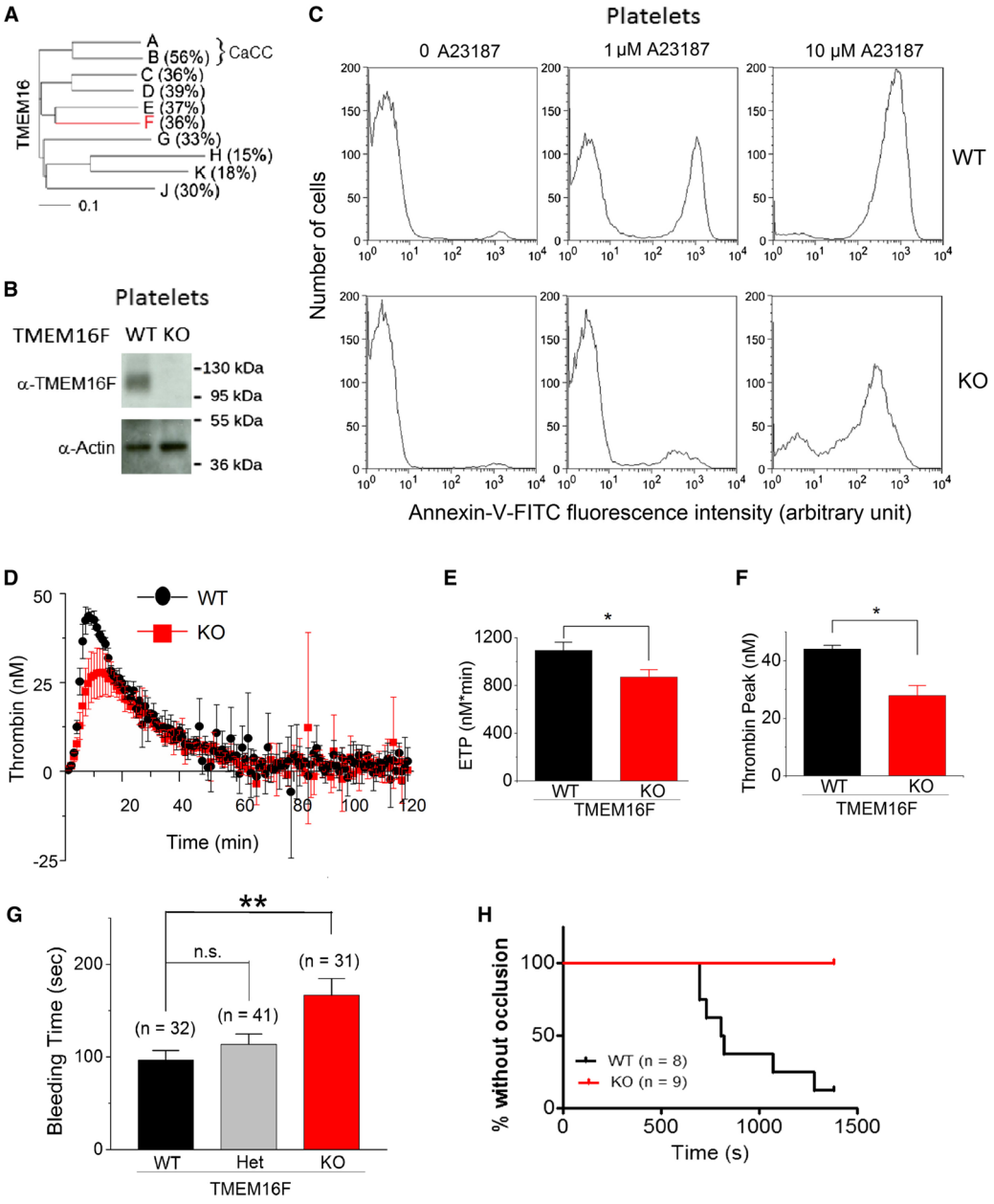

Figure 1. TMEM16F Knockout Mice Exhibit Deficiencies in Ca^{2+}-Dependent Scramblase Activity in Platelets, Defects in Blood Coagulation, and Protection against $FeCl_3$-Induced Carotid Thrombosis

(A) Phylogenetic tree of the human TMEM16 family generated by ClustalW2 with default settings. Percentage of amino acid identity with TMEM16A is indicated in parentheses. Scale bar, 0.1 nucleotide substitutions per site.

(B) Immunoblot analysis of TMEM16F expression in the platelets of wild-type (WT) and TMEM16F KO mice.

(C) Flow cytometry analysis of platelets from WT and TMEM16F KO mice treated with 0, 1, and 10 μM A23187 and FITC-Annexin-V for 30 min.

(D) Tissue-factor-induced thrombin generation curves for WT and TMEM16F KO mice.

(E) Endogenous thrombin potential (ETP, the area under the thrombin generation curve) of platelets from WT and TMEM16F KO mice induced by tissue factor. *$p < 0.05$. Error bar represents SEM.
(F) Thrombin generation peak height from the thrombin generation curves induced by tissue factor. *$p < 0.05$. Error bar represents SEM.
(G) Bleeding time measured by a hemostatic challenge assay. **$p < 0.005$. n.s., not significant. Error bar represents SEM.
(H) Carotid artery thrombosis by the 4% $FeCl_3$ injury model. Flow versus time after $FeCl_3$ application is shown. $p = 0.0002$ log rank test.
See also Figure S1.

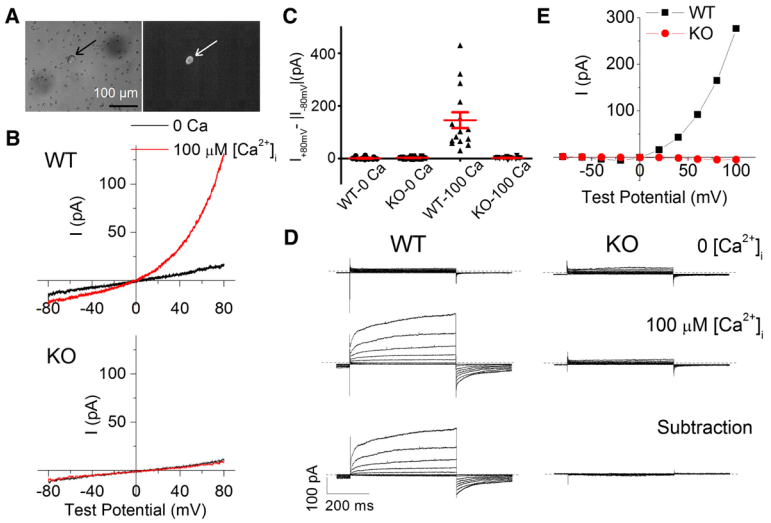

Figure 2. A Ca^{2+}-Activated, Outwardly Rectifying Current Present in Megakaryocytes of WT Mice Was Eliminated from TMEM16F KO Mice

(A) Megakaryocytes are CD41+ and morphologically distinct from the other cell types in the mouse bone marrow.

(B) Representative macroscopic current traces of inside-out patches excised from megakaryocytes of WT mice (top) and TMEM16F KO mice (bottom). The patches were exposed to 100 μM $[Ca^{2+}]_i$ with symmetrical 140 mM NaCl. The currents were elicited by voltage ramps from −80 to +80 mV with a rate (dV/dt) = 0.36 V/s.

(C) A Ca^{2+}-sensitive, outwardly rectifying current was observed in megakaryocytes of WT mice, but not TMEM16F KO mice ($p < 0.0001$). I_{+80mV} and $|I_{-80mV}|$ are the absolute values of current amplitudes at +80 and −80 mV, respectively. n equals 15 for WT and 14 for TMEM16F KO. Error bar represent SEM.

(D) Representative macroscopic current traces of inside-out patches excised from megakaryocytes of WT (left) and TMEM16F KO (right) mice in the absence or presence of 100 μM $[Ca^{2+}]_i$. Ca^{2+}-induced currents that were derived by subtracting the currents recorded with 0 $[Ca^{2+}]_i$ from the currents recorded with 100 μM $[Ca^{2+}]_i$ are shown at the bottom. Testing potentials were from −80 mV to +100 mV with 20 mV increments. Both holding and repolarizing potentials were −80 mV. Dotted lines indicate the zero current level. Both sides of the membrane patch were exposed to 140 mM NaCl solutions.

(E) *I-V* relationship of the subtracted peak current as shown in (D).

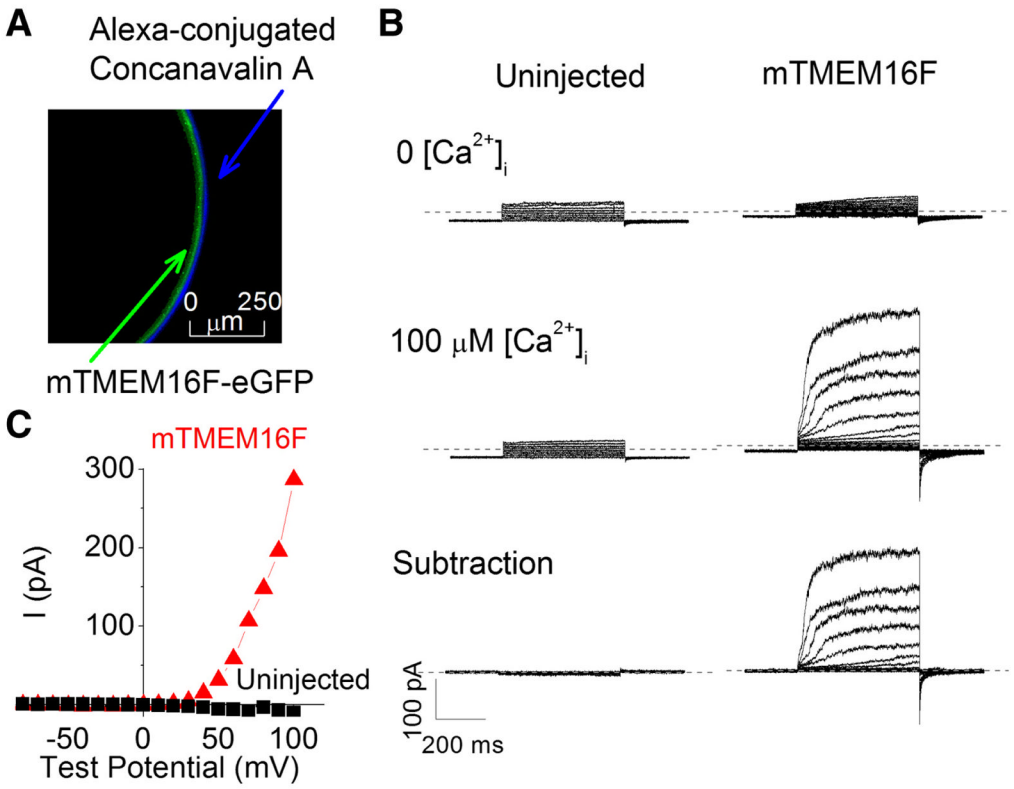

Figure 3. Functional Expression of TMEM16F in Axolotl Oocytes Elicits a Ca^{2+}- and Voltage-Dependent Current that Resembles the Endogenous TMEM16F Current in Megakaryocytes of WT Mice

(A) Surface expression of murine TMEM16F (mTMEM16F)-eGFP in an Axolotl oocyte. The eGFP signal (green) in the representative confocal image is in close proximity to the signal for Alexa-633-conjugated Concanavalin A (blue), which selectively binds to glycoproteins in the vitelline membrane of the Axolotl oocyte.

(B) Representative macroscopic current traces of inside-out patches excised from uninjected and mTMEM16F-expressing Axolotl oocytes in the absence or presence of 100 μM $[Ca^{2+}]_i$. Ca^{2+}-induced currents that were derived by subtracting the currents recorded with 0 $[Ca^{2+}]_i$ from the currents recorded with 100 μM $[Ca^{2+}]_i$ are shown at the bottom. Testing potentials were from −80 mV to +100 mV with 10 mV increments. Both holding and repolarizing potentials were −80 mV. Dotted lines indicate the zero current level. Both sides of the membrane patch were exposed to 140 mM NaCl solutions.

(C) *I-V* relationship of the subtracted peak current shown in (B).

See also Figure S2.

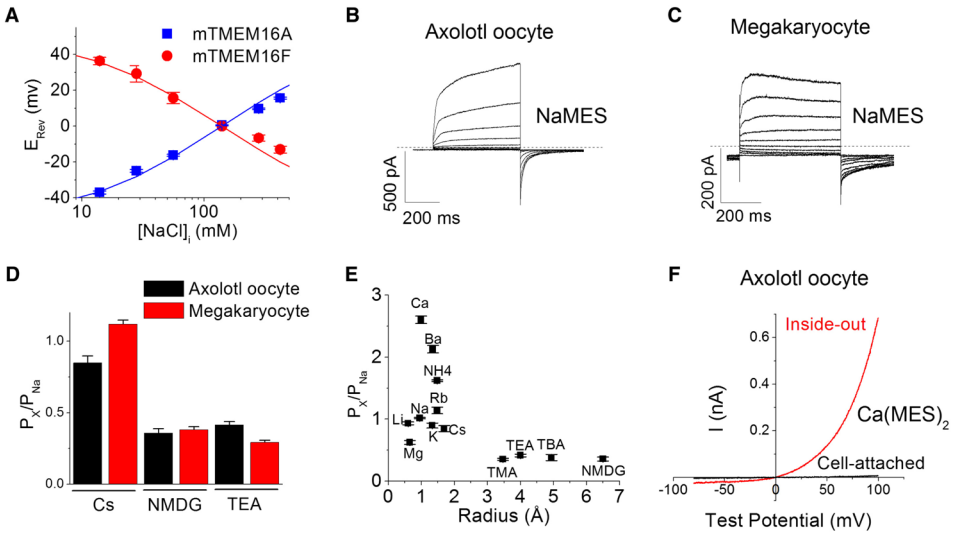

Figure 4. TMEM16F Encodes a Ca^{2+}-Activated, Nonselective Cation Channel Rather Than a CaCC

(A) Reversal potential (E_{Rev}) of mTMEM16A (m16A) and mTMEM16F (m16F) channels as a function of $[NaCl]_i$. E_{Rev} was measured as a function of $[NaCl]_i$ for channels recorded from inside-out patches, as shown in Figures S3A and S3B. The extracellular concentration of NaCl was kept constant at 140 mM. The solid lines were calculated according to the Goldman-Hodgkin-Katz (GHK) equation $\Delta Erev = 59\times\log[(P_{Na}\times[Na]_o + P_{Cl}\times[Cl]_i)/(P_{Na}\times[Na]_i + P_{Cl}\times[Cl]_o)]$ with $P_{Na}/P_{Cl} = 6.7$ for mTMEM16F and $P_{Na}/P_{Cl} = 0.14$ for mTMEM16A, wherin $[Na]_o$, $[Cl]_o$, $[Na]_I$, and $[Cl]_i$ are extracellular and intracellular Na^+ and Cl^- concentrations, respectively. n = 6–14. Error bar represents SEM.

(B and C) Representative inside-out patch-clamp recordings from Axolotl oocytes expressing mTMEM16F (B) and megakaryocytes of WT mice (C) with symmetrical 140 mM NaMES. The membrane patches were exposed to 100 μM $[Ca^{2+}]_I$, and testing potentials were from −80 mV to +100 mV with 20 mV increments. Both holding and repolarizing potentials were −80 mV.

(D) Both heterologously expressed mTMEM16F channels and endogenous TMEM16F channels in megakaryocytes are nonselective for cations. The relative cation permeability (P_X/P_{Na}) was calculated according to the GHK equation: $\Delta Erev = 59\times\log[(P_{Na}\times[Na]_o)/(P_X\times[X]_i)]$, in which ΔE_{Rev} values were measured as shown in Figures S3C–S3F. n = 6–13. Error bar represents SEM.

(E) Ionic radius versus relative cation permeability for the mTMEM16F channel expressed in Axolotl oocytes. The ΔE_{Rev} values were obtained from the bi-ionic conditions with 140 mM NaMES in the pipette solution and were used to calculate relative permeabilities according to the GHK equation. TMA, tetramethylammonium; TEA, tetraethylammonium; TBA, tetra-butylammonium; NMDG, N-Methyl-D-glucamine. All of the intracellular solutions contained 500 μM $[Ca^{2+}]_i$. n = 6–31. Error bars represent SEM.

(F) mTMEM16F channels are Ca^{2+} permeable. Currents were recorded before and after excision of inside-out membrane patches from mTMEM16F-expressing Axolotl oocytes into 70 mM $Ca(MES)_2$ bath solution. The extracellular bath solution contained 70 mM $Ca(MES)_2$. The *I-V* relationships were determined by voltage ramps from −80 to +100 mV with a rate (dV/dt) = 0.36 V/s.

See also Figures S3 and S4.

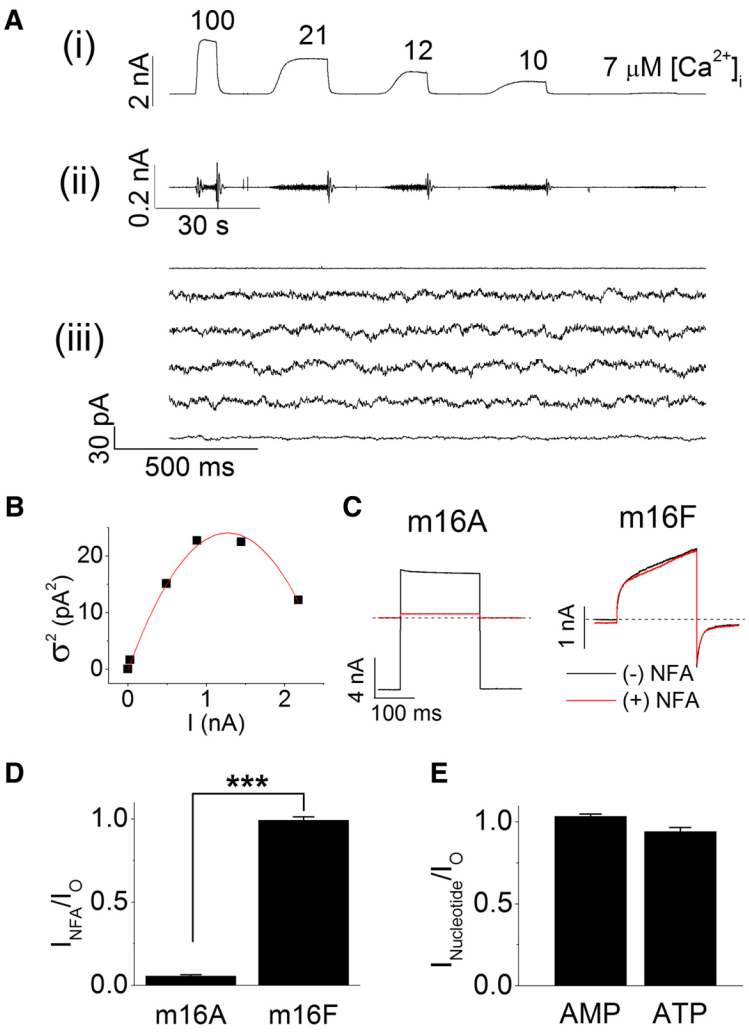

Figure 5. mTMEM16F Gives Rise to Small-Conductance Ca^{2+}-Activated, Nonselective Cation Channels with Distinct Pharmacological Properties

(A) Noise analysis of mTMEM16F currents expressed in HEK293 cells. (i) Representative current traces recorded in the presence of various $[Ca^{2+}]_i$ at +80 mV. (ii) 2 Hz high-pass-filtered current traces shown in (i). (iii) Enlarged high-pass-filtered current traces with 2 s duration under each $[Ca^{2+}]_i$.

(B) The variance of the current traces shown in (A) was plotted against the current amplitudes and fitted with $\sigma^2 = iV_m\gamma - \bar{I}^2/N$. The obtained fitting parameters were γ = 0.47 pS and N = 67,006. The averaged channel conductance obtained from 15 different patches was γ = 0.45 ± 0.07 pS.

(C) 300 μM intracellular niflumic acid (NFA) blocked most of the mTMEM16A Cl^- currents, but not the mTMEM16F Na^+ currents. Inside-out patches from Axolotl oocytes were exposed to symmetrical 140 mM NaCl and 100 μM $[Ca^{2+}]_i$ for mTMEM16A and symmetrical 140 mM NaMES and 100 μM $[Ca^{2+}]_i$ for mTMEM16F. Currents were elicited by voltage pulses stepped from 380 to +80 mV.

(D) Summary of the NFA effects shown in (C). I_{NFA} and I_O are the maximum peak current amplitudes in the presence and absence of NFA, respectively. n = 7–8. ***p < 0.0001. Error bars represent SEM.

(E) 2 mM free $[AMP]_i$ and $[ATP]_i$ had little effect on the mTMEM16F currents. Inside-out patches from Axolotl oocytes were exposed to symmetrical 140 mM NaMES, 100 μM $[Ca^{2+}]_I$, and AMP or ATP. I_O is the maximum current amplitude in the absence of the nucleotides. n = 6–7. Error bar represents SEM.
See also Figure S5.

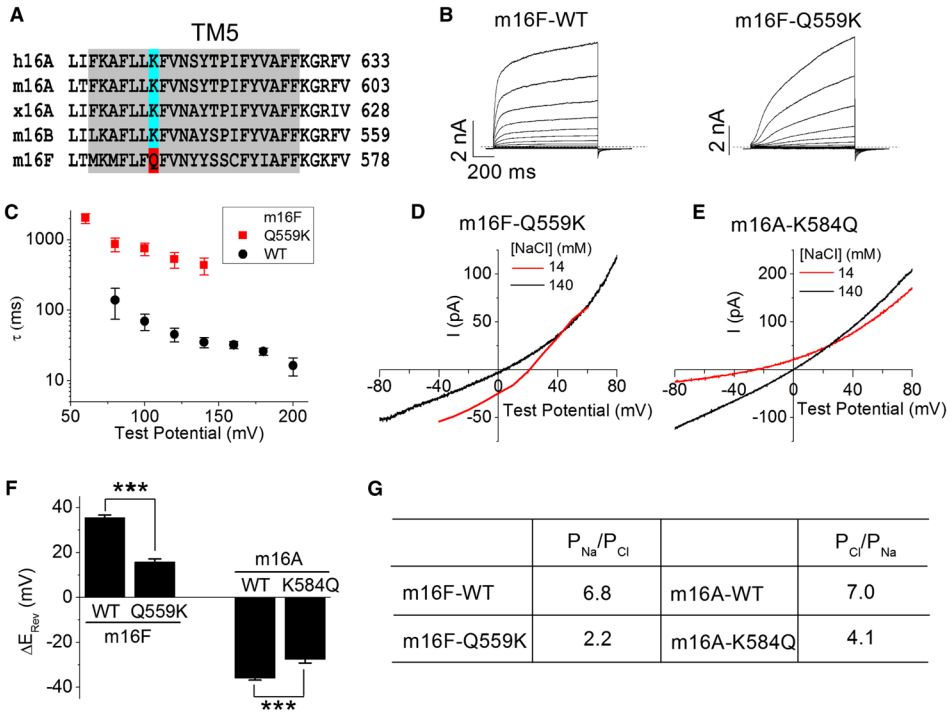

Figure 6. A Residue in the Transmembrane Segment 5 Is Important for the Ion Selectivity of mTMEM16F-SCAN and mTMEM16A-CaCC Channels

(A) Sequence alignment of the transmembrane segment 5 (TM5) of human TMEM16A (h16A), murine TMEM16A (m16A), *Xenopus* TMEM16A (x16A), murine TMEM16B (m16B), and murine TMEM16F (m16F).

(B) Representative macroscopic current traces of WT and Q559K mutant mTMEM16F channels expressed in HEK293 cell. The inside-out patches were exposed to 100 μM $[Ca^{2+}]_i$ and symmetrical 140 mM NaCl. Testing potentials were from −80 mV to +180 mV with 20 mV increments. Both holding and repolarizing potentials were –80 mV.

(C) Semi-log plots of mean activation time constants (τ) as a function of voltage for the WT and Q559K-mTMEM16F channels. t was derived from the single exponential fitting of the current traces shown in (B). n = 5–7. Error bar represents SEM.

(D and E) Representative *I-V* relationships of the Q559K-mTMEM16F (D) and K584Q-mTMEM16A (E) mutant channels recorded from inside-out patches exposed to 14 and 140 mM $[NaCl]_i$ and 500 μM $[Ca^{2+}]_i$.

(F and G) Summary of the reversal potential shift (ΔE_{Rev}) (F) and relative ion permeability (G) for the WT and mutant channels when $[NaCl]_i$ switched from 140 mM to 14 mM. n = 8–19. ***p < 0.0001. Error bar represents SEM.

All of these experiments were recordings from inside-out membrane patches from HEK293 cells.

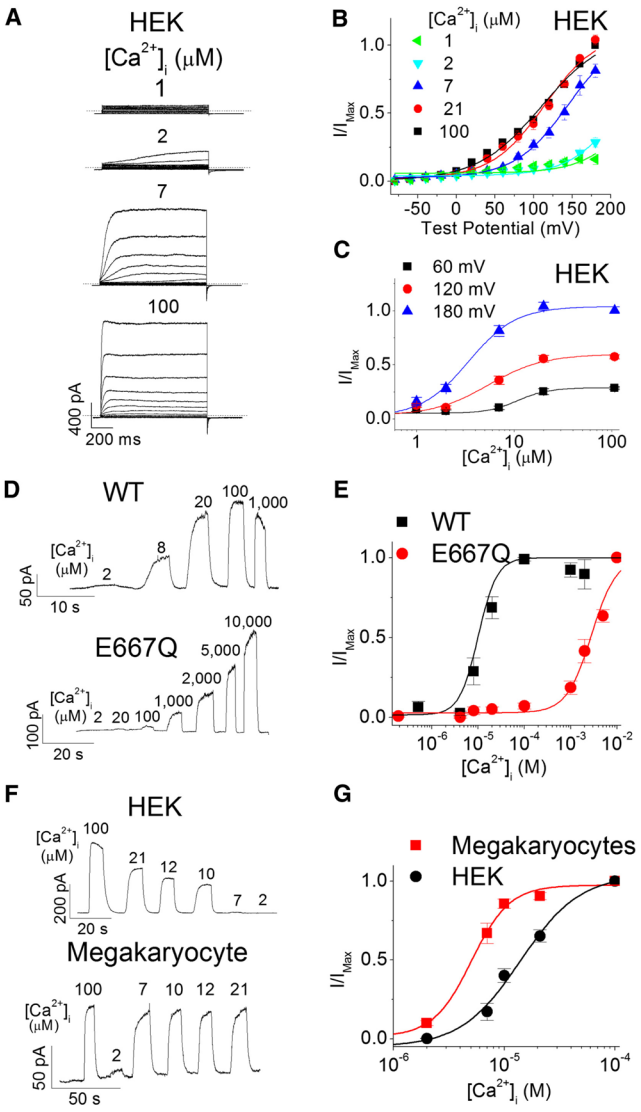

Figure 7. Gating of Heterologously Expressed mTMEM16F and Endogenous TMEM16F Channels in Megakaryocytes Is Ca^{2+} and Voltage Dependent

(A) Representative macroscopic current traces of an inside-out patch excised from a mTMEM16F-expressing HEK293 cell exposed to 1, 2, 7, and 100 μM $[Ca^{2+}]_i$. Testing potentials were from −80 mV to +180 mV with 20 mV increments. Both holding and repolarizing potentials were −80 mV.

(B) Mean *G-V* relations of the mTMEM16F channels under different $[Ca^{2+}]_i$. Relative conductance was determined by measuring the amplitude of tail currents 400 μs after repolarization to a fixed membrane potential (−80 mV). The smooth curves represent Boltzmann fits $I/I_{Max} = 1/(1 + \exp(-ze(V - V_{1/2})/kT))$ (see Table S1). I_{Max}, tail current amplitude in response to deploarizaton to +180 mV in 100 μM $[Ca^{2+}]_i$. Error bar represents SEM.

(C) Ca^{2+} dose-response of the mTMEM16F channel at +60, +120, and +180 mV. I/I_{Max} values were from (B). The smooth curves represent the fits to the Hill equation: $I/I_{Max} = Amp/(1 + (K_D/[Ca])^H)$, wherein K_D is the apparent dissociation constant, H is the Hill coefficient, and Amp is the maximum value of I/I_{Max} at certain voltage. +60 mV: (K_D =

10.8 ± 4.6 μM, H = 2.8); +120 mV: (K_D = 5.4 ± 1.6 μM, H = 1.5); +180 mV: (K_D = 3.4 ± 0.5 μM, H = 1.8). n = 5–21. Error bar represents SEM.

(D) Representative inside-out patch-clamp recordings of WT (top) and E667Q mutant (bottom) mTMEM16F channels expressed in HEK293 cells. The membrane patches were voltage clamped at +60 mV and exposed to different $[Ca^{2+}]_i$.

(E) Comparison of Ca^{2+} sensitivity between the WT and E667Q mutant TMEM16F channels at +60 mV. The smooth curves represent the fits to the Hill equation. WT: K_D = 13.6 ± 1.8 μM, H = 2.2 ± 0.5; E667Q: K_D = 2.8 ± 0.3 mM, H = 1.6 ± 0.3. n = 11–17. Error bar represents SEM.

(F) Representative inside-out patch-clamp recordings from the mTMEM16F-expressing HEK293 cells (top) and megakaryocytes of WT mice (bottom). The membrane patches were voltage clamped at +60 mV and exposed to different $[Ca^{2+}]_i$.

(G) Comparison of the Ca^{2+} sensitivity of the endogenous TMEM16F-SCAN current in megakaryocytes with that of the heterologously expressed TMEM16F channels in HEK293 cells at +60 mV. The smooth curves represent the fits to the Hill equation. For mTMEM16F currents in HEK293 cells, K_D = 13.9 ± 2.9 μM, H = 1.6; for endogenous TMEM16F currents in megakaryocytes, K_D = 5.1 ± 2.0 μM, H = 2.5. n = 6–12. Error bar represents SEM.

All experiments were recordings from inside-out membrane patches in symmetrical 140 mM NaMES solutions except for the experiments shown in (D) and (E), which were done in symmetrical 140 mM NaCl solutions.

See also Figure S6 and Table S1.